LANGMUIR Article
Cite This: Langmuir 2019, 35, 17000−17008
pubs.acs.org/Langmuir

Theoretical and Experimental Studies on the Controllable Pancake Bouncing Behavior of Droplets

Huaping Wu,*,† Kunpeng Jiang,† Zhenxiong Xu,† Sihang Yu,† Xiang Peng,† Zheng Zhang,† Hao Bai,‡ Aiping Liu,§ and Guozhong Chai†

†Key Laboratory of E&M, Zhejiang University of Technology, Ministry of Education & Zhejiang Province, Hangzhou 310014, China

‡State Key Laboratory of Chemical Engineering, College of Chemical and Biological Engineering, Zhejiang University, Hangzhou 310027, China

§Center for Optoelectronics Materials and Devices, Zhejiang Sci-Tech University, Hangzhou 310018, China

Supporting Information

ABSTRACT: A droplet that impacts on a superhydrophobic surface will undergo a process of unfolding, contracting, and finally rebounding from the surface. With regards to the pancake bouncing behavior of a droplet, since the retraction process of the droplet is omitted, the contact time is greatly shortened compared to the normal type of bouncing. However, the quantitative prediction to the range of droplet pancake bouncing and the adjustment of pancake bouncing state have yet to be probed into. In this paper, we reported the controllable pancake bouncing of droplets by adjusting the size of the superhydrophobic surface with microstructures. In addition, we also discovered a dimensional effect with regards to pancake bouncing, namely, the pancake bouncing would be more likely to happen on the surfaces with large post spacing for the droplet with the larger radius. The contact time could be reduced to 2 ms by adjusting the size of the microstructures and the radius of the droplets. Based on the relationship between the droplet bouncing state and the surface microstructure size, we are able to propose reasonable dimensions for the surfaces in order to control pancake bouncing.

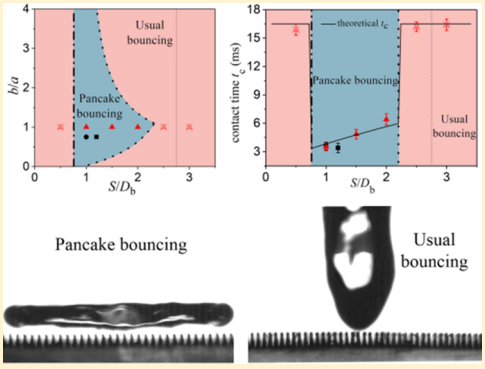

INTRODUCTION

Research related to the dynamic wettability of solid material surfaces has attracted much attention, especially for the investigation concerning the reduction of liquid−solid contact time.[1−6] The ability of droplets to rapidly bounce on the surface is of great importance to industrial applications, particularly with regards to the surface with self-cleaning, anti-corrosion, and icing resistance.[7−19] When a droplet impacts on a superhydrophobic surface, it will first spread to a maximum diameter on the solid surface, then retract, and finally leave the substrate or stick to it through heterogeneous surface wettability regulation.[20−25] It has been reported that the contact time in the spreading stage is independent of the substrate's microstructure or droplet's impact velocity.[26−28] In order to reduce the contact time of the droplets with the surface, shortening the contact time of droplets in the retracting stage is the key.

Methods of shortening the contact time of the droplets with the surface can be roughly divided into three types. From the perspective of redistributing liquid quality, Bird et al.[29] reduced the contact time of the droplet by nearly 37% compared to control experiments by splitting the droplet into two parts during the retracting stage.[30,31] Liu et al.[32] found that droplets rebounded from the Echeveria surface with distinctly different retraction rates along two perpendicular directions. The asymmetry of the droplets' bouncing lead to a 40% reduction in contact time, which was primarily driven by an asymmetric momentum transfer on the cylindrical leaves.[33] Additionally, the contact time of the droplets can also be shortened via capillary forces, that is, the liquid infiltrates the microstructures and pushes the droplets upwards.[34,35] In this case, the retraction process of the droplets is mitigated, and the droplets rebound from the surface in the shape of a pancake. It has been reported that the pancake bouncing of droplets can be observed on anisotropic surfaces, superhydrophobic meshes, and superhydrophobic conical array surfaces (SCASs).[36,37] The contact time of the droplets rebounding on the superhydrophobic cone arrays was reduced by nearly 80%, which was the reported shortest contact time.[34] Furthermore, the sizes of the microstructures and the droplets, the elastic substrate, and triple contact line pinning can also affect the pancake bouncing.[38−43] Although many research groups are

Received: October 10, 2019
Revised: November 6, 2019
Published: December 1, 2019

DOI: 10.1021/acs.langmuir.9b03153
Langmuir 2019, 35, 17000−17008

still studying the pancake bouncing of droplets,[44−46] a reliable and suitable method to achieve pancake bouncing is necessary to be proposed, which will be helpful for controlling the rapid detachment of droplets from the surface.

In this paper, we focus on the dynamic rebound behavior of droplets on microstructured surfaces with different sizes and the relation between the droplet size and pancake bouncing state. We first analyzed the wettability of the surface with superhydrophobic tapered arrays using a thermodynamic approach and the principle of minimum free energy, and three constraints that must be satisfied were listed to achieve the pancake bounce of droplets. Next, the accuracy of the theoretical derivation was verified experimentally by comparing the bouncing states of droplets on the SCAS with different microstructure sizes, and the influence of the microstructure size on the contact time was analyzed. Finally, in rebound experiments related to the droplet sizes, we found that smaller droplets were more suitable for pancake bouncing on surfaces with denser microstructure spacing, and reducing the volume of the droplet could shorten the pancake bouncing time. The report focuses on the pancake bouncing caused by the low-speed impact of droplets, and droplets will not splash before detaching from the surface in this range. In general, our purpose is to find a solution for adjusting the rebound behavior of droplets and providing a reference for a microstructure surface design under different working conditions.

THEORETICAL BASIS

The Wettability of the Surface. The rebound behavior of the droplet on a surface with a tapered microstructure is very significant,[34,36,37] which is also more susceptible to superhydrophobic surfaces. Therefore, we first analyze the wettability of the SCAS with the conical array height H, top surface diameter D_t, bottom surface diameter D_b, half apex angle of the tapered column α, and bottom spacing between two posts S, as shown in the schematic diagram (Figure 1).

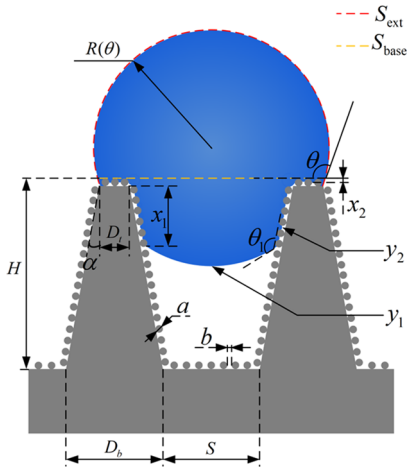

Figure 1. Schematic of a droplet on the superhydrophobic conical array surface (SCAS).

Furthermore, the surface of the conical posts is uniformly covered with a layer of a nanosphere with a diameter a and spacing b. The radius of the droplet is $R(\theta)$, the outer surface area of the spherical droplet is S_{ext}, and the cross-sectional area in contact with the microstructure is S_{base}. The contact angles of the droplets on the surface with two microstructures are θ and θ_1, the depths of infiltration are x_1 and x_2, and the ratios of the area of the droplet to the projected area on the corresponding surface are y_1 and y_2. S/D_b is defined as the ratio between the spacing of the conical arrays and the diameter of the posts' underside, and b/a is the ratio of the pitch between the nanosphere structures and the diameter.

In our previous studies, a thermodynamic approach and the principle of minimum free energy were used to analyze the wetting states of a droplet on a microstructured surface.[47,48] Ordinarily, a droplet has two stable wetting states (Cassie−Baxter and Wenzel) on the surface with a single-scale microstructure. The wetting states are usually more complicated for the droplet on dual-scale rough surfaces. It is assumed that the droplets possess four stable wetting states on the SCAS, namely CB−CB (conical arrays and nanospheres are all in Cassie−Baxter states), CB−W (conical arrays are in a Wenzel state, and the nanospheres are in a Cassie−Baxter one), W−CB (conical arrays are in a Cassie−Baxter state, and the nanospheres are in a Wenzel one), and W−W (conical arrays and nanospheres are all in Wenzel states). The corresponding equations of the apparent contact angle θ are demonstrated in Table 1, where θ_0 is the intrinsic contact angle on the SCAS. The specific derivation details of the formula are demonstrated in the C1 Section in the Supporting Information.

Table 1. Apparent Contact Angle Equations of Four Wetting States on the SCAS

wetting state	apparent contact angle equation
CB−CB	$\cos\theta_{CB-CB} = \frac{\pi(D_t/2)^2}{(S+D_b)^2}\frac{\pi a^2}{3(a+b)^2}\cos\theta_0 + \frac{\pi(D_t/2)^2}{(S+D_b)^2}\frac{2\pi a^2}{9(a+b)^2} - 1$
CB−W	$\cos\theta_{CB-W} = \left[\frac{(S+D_b)^2 - \pi(D_b/2)^2 + \pi(D_t/2)^2 + 0.5\pi(D_t+D_b)(H/\cos\alpha)}{(S+D_b)^2}\right] \times \left[\frac{\pi a^2}{3(a+b)^2}\cos\theta_0 + \frac{2\pi a^2}{9(a+b)^2} - 1\right]$
W−CB	$\cos\theta_{W-CB} = \frac{\pi(D_t/2)^2}{(S+D_b)^2}\left[1 + \frac{\pi a^2}{(a+b)^2}\right]\cos\theta_0 + \frac{\pi(D_t/2)^2}{(S+D_b)^2} - 1$
W−W	$\cos\theta_{W-W} = \frac{(S+D_b)^2 - \pi(D_b/2)^2 + \pi(D_t/2)^2 + 0.5\pi(D_t+D_b)(H/\cos\alpha)}{(S+D_b)^2} \times \left[1 + \frac{\pi a^2}{(a+b)^2}\right]\cos\theta_0$

According to the principle of thermodynamics and minimum free energy, the numerical values of the free energy of the four wetting states under different sizes (S/D_b and b/a) are calculated, and the state with the smaller free energy is selected as the stable state, as shown in Figure 2a. According to previous studies, the CB−W region is called as the "Petal effect" region, which exhibits a strong adhesive force to water, whereas the CB−CB region corresponds to low contact angle hysteresis, and is called as the "Lotus effect".[49] In order to reduce the energy loss of the droplet during the rebound, the Lotus effect region instead of the Petal effect one should be aimed. Consequently, by reasonably adjusting the parameter of microstructures (S/D_b and b/a), the droplets can be mostly controlled in the CB state (Figure 2a). Similarly, Figure 2b presents the wetting phase diagram of H and S/D_b. This indicates that the conical posts require a certain height to keep the droplets in the CB−CB region.

Rebound Energy of the Droplets. Throughout the whole bouncing process, the total energy of the system is conserved. The initial energy of the droplet W_{total} can be

DOI: 10.1021/acs.langmuir.9b03153
Langmuir 2019, 35, 17000−17008

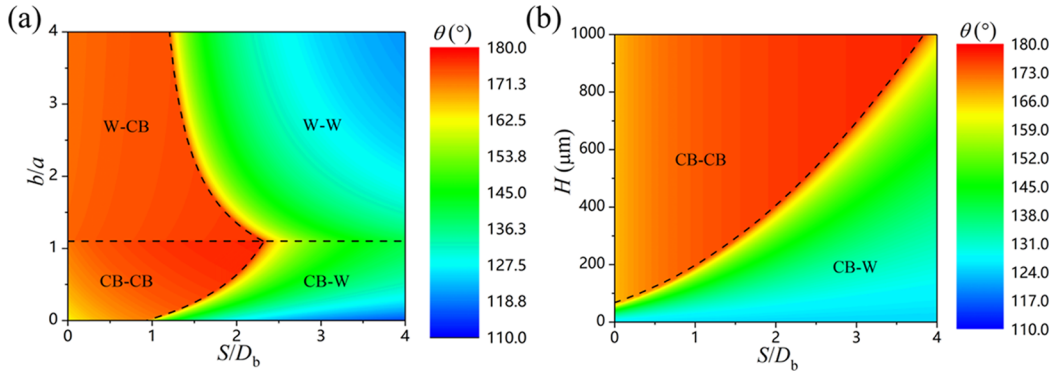

Figure 2. Wetting phase diagram of a droplet on the SCAS with (a) different S/D_b and b/a, (b) different H and S/D_b. S/D_b is defined as the ratio between the spacing of the conical arrays and the diameter of the posts' underside, b/a is the ratio of the pitch between the nanosphere structures and the diameter, H is the height of posts. The dashed lines indicate that two adjacent wetting states have same apparent contact angles.

expressed by its gravitational potential energy and surface energy, and can be determined by

$$W_{total} = mgh + 4\pi R_0^2\gamma = 4\rho\pi R_0^3 gh/3 + 4\pi R_0^2\gamma \quad (1)$$

where m, γ , ρ , h and R_0 are the mass, surface tension, density, drop height, and the initial radius of the droplets, respectively.

We assume that the drop can jump as a pancake, with a maximum spreading diameter $D_{max} = \xi D_0 We^{1/4}$[50,51] and height h_{max}, where the prefactor ξ is close to unity. The Weber number can be expressed as $We = \rho v_0^2 R_0/\gamma$, where v_0 is the impact velocity at which the droplet contacts the top surface. D_0 is the initial diameter of the droplets. h_{max} can be expressed by volume conservation. Therefore, when the droplets leave the surface as a pancake, the interface energy E_s can be expressed as $E_s = (\pi D_{max}^2/2 + \pi D_{max} h_{max})\gamma$, and the final kinetic energy is defined as E_f. The liquid friction against the pillars during the spreading process is scaled as[52]

$$F_1 \approx \frac{\mu V H_x D}{(S + D_b)^2\left[\ln\left(\frac{S + D_b}{D_a/2}\right) - 1.31\right]} \quad (2)$$

According to the literature,[8] the penetrating distance of liquid is approximately equivalent to the initial drop diameter. Therefore, the distance D of the liquid front is approximately equal to $D_0/2$. μ is the viscosity, H_x is the penetration depth, and V is the averaged velocity, which can be expressed as $V = D_0/\tau$ where $\tau = D_0/v_0$ is the characteristic time. D_a is the average diameter of the pillar, which can be expressed as $D_a = (D_b + D_t)/2$. The energy dissipation by liquid fraction against the pillars during spreading and receding is expressed as[53]

$$W_1 = \frac{\pi^2\mu H_x D_0^3 v_0}{3(S + D_b)^2\left[\ln\left(\frac{S + D_b}{D_a/2}\right) - 1.31\right]} \quad (3)$$

The liquid friction from the bottom is expressed as[53]

$$F_2 = \pi\mu\frac{V}{H}\frac{D^2}{2} \quad (4)$$

and the energy dissipation by liquid fraction against the bottom during spreading and receding is expressed as

$$W_2 = \frac{\pi\mu D_0^3 v_0}{6H} \quad (5)$$

The viscous dissipative energy of the droplet against the pillars' top is expressed as[54]

$$W_3 = \frac{\pi}{8}\mu v_0 D_{max}^2 f_s\sqrt{Re} \quad (6)$$

Here, f_s is the fraction of the liquid−solid contact area, which can be expressed as $f_s = \pi(D_t/2)^2/(S + D_b)^2$, and Re is the Reynolds number, which can be expressed as $Re = \rho D_0 v_0/\mu$.

The energy conservation between the initial stage and the final stage can be expressed as $W_{total} = E_f + E_s + W_1 + W_2 + W_3$. In order to allow the droplets to bounce off the surface, it is necessary that the final kinetic energy $E_f \geq 0$, and therefore[45]

$$W_{total} - W_1 - W_2 - W_3 \geq E_s. \quad (7)$$

The Timescale of Pancake Bouncing. We determine the time interval between the first contact of the droplet to the surface and the complete emptying of the substrate as $t_\uparrow$, the time when the droplet reaches its maximum lateral extension as t_{max}, and the ratio of them as $k = t_\uparrow/t_{max}$. According to the research of Liu et al.,[34] pancake bouncing occurs at $0.5 < k < 1.7$ on the SCAS. The maximum lateral extension time t_{max} can be expressed as[36,38]

$$t_{max} \sim \sqrt{\rho R_0^3/\gamma} \quad (8)$$

with a fitting coefficient of 0.62. When the droplet can touch the bottom surface, the $t_\uparrow$ can be split into three parts and expressed as $t_\uparrow = t_{down} + t_{touch} + t_{up}$, namely, the sum of falling time t_{down}, touching time t_{touch}, and rising time t_{up}.[36] For tapered posts, the acceleration is linear with penetration depth. The capillary force F_{cf} can be approximately expressed as $F_{cf} = n\pi\gamma(D_t + 2x\tan\alpha)\cos\alpha\sin(\theta_1 - 90^\circ)$[55] during filling, which is given by $-F_{cf} = m^*d^2x/dt^2$, and the boundary conditions are expressed as $(dx/dt)_{t=0} = v_0$ and $x_{t=0} = 0$, where x is the penetration depth. Then, the falling time of the droplet can be obtained as

$$t_{down} = \sqrt{\frac{m^*}{k}}\arccos\left[\frac{F_{f0}^2 + F_{f0}H_x k + k v_0\sqrt{(m^*)^2 v_0^2 - 2F_{f0}H_x m^* - H_x^2 k m^*}}{F_{f0}^2 + k m^* v_0^2}\right] \quad (9)$$

with $F_{f0} = n\pi\gamma D_t\cos\alpha\sin(\theta_1 - 90^\circ)$ and $k = 2n\pi\gamma\tan\alpha\cos\alpha\sin(\theta_1 - 90^\circ)$. m^* is the effective mass, which can be expressed as $m^* = f_t m$. $v_{(Hx)}$ is the velocity of the droplet when reaching the maximum penetration depth H_x, which can be

DOI: 10.1021/acs.langmuir.9b03153
Langmuir 2019, 35, 17000−17008

expressed as $v_{(Hx)} = \sqrt{v_0^2 - 2H_xF_{f0}/m^* - H_x^2k/m^*}$. H_x is determined via the boundary condition $v_{(Hx)} = 0$ as

$$H_x = \begin{cases} H & x \geq H \\ \dfrac{\sqrt{F_{f0}^2 + km^*v_0^2} - F_{f0}}{k} & x < H \end{cases} \quad (10)$$

where $n = \pi R_0^2/(S + D_b)^2$ is the number of posts covered by the penetrating liquids.

When the droplet does not touch the bottom surface, $v_{(Hx)} = 0$ and $t_{touch} = 0$. However, if the droplet touches the bottom surface, the total reactive force acting on the droplet contains the capillary force F_c and the force from the bottom substrate F_b. According to the momentum conservation law, $F_b = m^*v_0/t_{max}$. Then, the total force can be expressed as $F_t = F_b + F_c$, where $F_c = n\pi\gamma D_b \cos\alpha \sin(\theta_1 - 90^\circ)$ when the droplet touches the bottom surface. Then, the touching time of the droplet can be obtained as

$$t_{touch} = m^*v_{(Hx)}/F_t \quad (11)$$

During emptying, the capillary force F_{ce} can be approximately expressed as $F_{ce} = n\pi\gamma(D_t + 2H_x\tan\alpha - 2y\tan\alpha)\cos\alpha \sin(\theta_1 - 90^\circ)$, which is given by $F_{ce} = m^*d^2y/dt^2$, and the boundary conditions are expressed as $(dy/dt)_{t=0} = 0$ and $y_{t=0} = 0$, where y is the emptying height. Then, the falling time of the droplet can be obtained as

$$t_{up} = \sqrt{\frac{m^*}{k}} \arccos\left[\frac{F_{e0} - H_xk}{F_{e0}}\right] \quad (12)$$

with $F_{e0} = n\pi\gamma(D_t + 2H_x\tan\alpha)\cos\alpha \sin(\theta_1 - 90^\circ)$.

Through experiments, we find that only part of the droplet mass affects the rebound effectively. We assume that the droplet mass is the same at all stages, and the scaling factor $f_t = 0.67$.[45] The effect of gravity, the Laplace pressure, and liquid friction on the vertical motion are neglected. According to the research of Liu et al.,[34] the contact time t_c is approximately equal to the $t_\uparrow$ over the pancake bouncing range. Using this theory, experimental values can be predicted relatively accurately.

EXPERIMENTAL SECTION

Substrate Preparation. For the preparation of the substrates, we predominantly used trimethoxyoctadecylsilane TMOS (Aladdin), titanium dioxide TiO_2 nanoparticles (anatase and rutile, <40 nm, 99.7% trace, Sigma Aldrich), and poly(dimethylsiloxane) PDMS (Dow Corning Sylgard 184). Additionally, a copper mold with a square lattice of tapered holes, with diameters of 100 μm and depth of 600 μm was used as a template. A brief experimental outline was displayed in Figure 3. First, the base polymer and the curing agent of PDMS were mixed at a mass ratio of 5:1 w/w. The bubbles were then removed from the PDMS before it was poured onto the copper template. After the PDMS was cured, it was carefully separated from the copper template to provide a surface with conical arrays. Next, the solution composed of TMOS, absolute ethanol (~99 wt%, Eagle Chemical Reagent Co., Ltd., Zhejiang), and TiO_2 was spin-coated on the surface of the conical arrays, and finally the substrate with SCAS was obtained.

Characterization. The surface morphology of the sample was observed with scanning electron microscopy (SEM, Hitachi S4800). In order to characterize the wettability of the SCAS, the water contact angle (CA, θ) was measured using 4 μL droplets of deionized water with a contact angle instrument (OCA 50AF, Dataphysics Instruments). The water droplets were dispensed using a syringe pump through a needle with a 100 μm inner diameter.

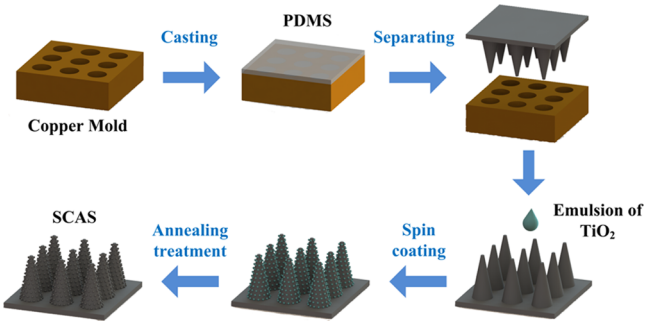

Figure 3. Schematic diagram of the preparation of a SCAS by the template method and spin-coating technology.

Figure 4a,b shows the SEM images of the conical arrays with $S/D_b = 1.0$ and the nanosphere structures, respectively. The SEM images of the SCAS with different microstructure spacings are also demonstrated in Figure S1 in the Supporting Information. The surface with $S/D_b = 1.0$ exhibits a superhydrophobic property with an apparent contact angle of 160 ± 1.0° (Figure 4c).

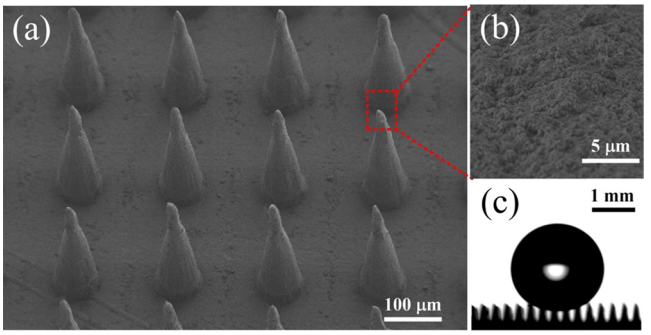

Figure 4. (a) SEM image of the conical arrays with $S/D_b = 1.0$. (b) SEM image of the nanosphere structures. (c) Apparent contact angle of SCAS with $S/D_b = 1.0$ is 160 ± 1.0°.

Droplet Impact. In the droplet impact experiments, the radius of the droplets was controlled by replacing the needles of the syringe with different inner diameters (R_0 = 0.89−2.6 mm) and adjusting the impact velocity v_0 of droplets by changing the release height h, corresponding to $0 < We < 50$. A high-speed camera (pco.dimax HD 900000587) was utilized to capture the details of the droplet impact at 10,000 frames per second. In all cases, the droplets were maintained at room temperature, and the indoor humidity was approximately 55%.

Droplet Bouncing Experiment. The impact experiment of the droplets was performed on the SCAS with the ratio of conical arrays S/D_b being 0.5, 1, 1.5, 2, 2.5, and 3. Specific geometrical parameters of the SCAS are displayed in Table S2 in the Supporting Information. Figure 5a−e shows selected snapshots of a droplet impacting on the SCAS with $R_0 = 1.45$ mm and $We = 16$. For surfaces with conical array ratios of $S/D_b = 0.5$ and $S/D_b = 2.5$, as shown in Figure 5a,e, the droplets undergo the usual rebound on the SCAS with a contact time t_c of approximately 15.5 ms, similar to the regular rebound in previous studies[23] $(2.55\sqrt{\rho R_0^3/\gamma})$. However, when the droplets impact on the surface with $S/D_b = 1$, 1.5, and 2, as shown in Figure 5b−d, the droplets rebound from the SCAS in the form of a pancake, which is termed as pancake bouncing of the droplets. In this case, the liquid penetrates into the microstructure and the drop detaches from the surface immediately after capillary emptying without retraction.[34] It can be seen that as the array spacing increases, the pancake bouncing time of the droplets also tends to increase. As the S/D_b increases from

DOI: 10.1021/acs.langmuir.9b03153
Langmuir 2019, 35, 17000−17008

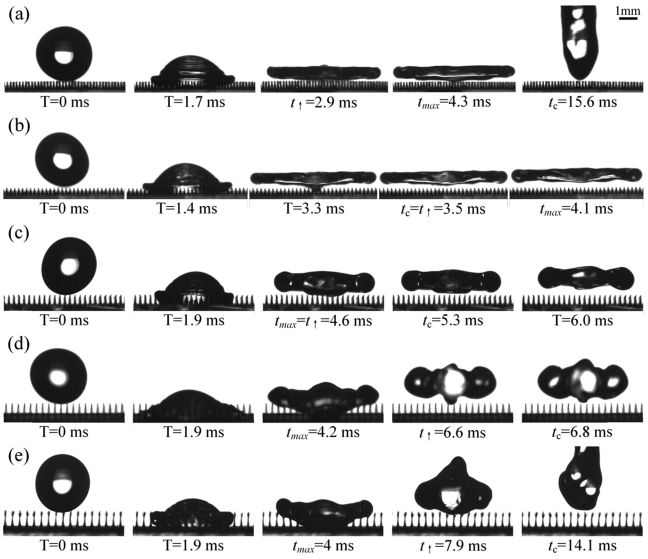

Figure 5. Selected snapshots of the droplet's rebounding behavior on the SCAS with (a) S/D_b = 0.5, (b) S/D_b = 1.0, (c) S/D_b = 1.5, (d) S/D_b = 2.0, and (e) S/D_b = 2.5. The droplet radius is R_0 = 1.45 mm at We = 16.

1 to 1.5 and then to 2, the t_c becomes 3.5, 5.3, and 6.8 ms, respectively, and the pancake shape appears when the droplet rebounds more irregularly (Videos S1–S5 in the Supporting Information). According to previous studies, it can be concluded that the following conditions should be satisfied when the pancake bouncing occurs for the droplet, namely: (i) wetting states become the Lotus effect region through an appropriate size, (ii) the energy criterion is satisfied, and (iii) an appropriate timescale k. The lack of any of these three will prevent pancake bouncing.[34]

RESULTS AND DISCUSSION

The Apparent Contact Angle of the Droplets. In order to analyze the wettability of the SCAS more intuitively, the relationship between the apparent contact angle θ and microstructural sizes was investigated. Figure S2 presents the wetting states of a droplet on the SCAS with different half-apex angles (S/D_b = 1). The θ can be improved by appropriately increasing the α of the tapered column. In Figure 6a, different colored lines represent the wetting states and θ of the droplets with different b/a, and the black solid points are the values obtained from previous experiments conducted by Chen and Bertola[33] and Liu et al.,[34,44] with ranges of b/a between 0.5 and 1.5 and between 0.5 and 1, respectively. In order to verify this

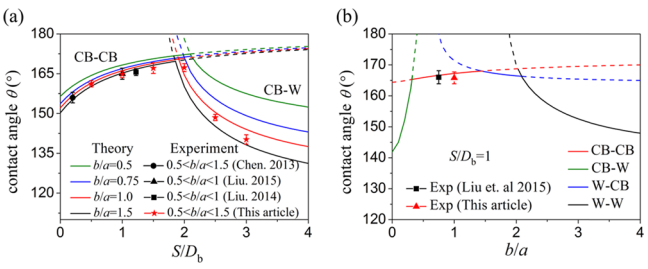

Figure 6. Wetting states of the droplet (R_0 = 1.45 mm) on the surface with different sizes of (a) conical arrays and (b) nanospheres. The black solid points on the graph are the experimental values of the previous experiments, and the red solid points are the experimental values reported in this research.

theory, the SCASs with different spacings (S/D_b) are studied, as shown by the red solid pointed line in the figure. Similarly, the estimated ratio b/a of the nanostructures is between 0.5 and 1.5. It can be seen that when the droplets are in a CB–CB state, the θ can be improved by appropriately increasing the S/D_b of the conical arrays. However, a very large spacing will result in the droplets being in the CB–W area. Furthermore, the nanospheres with different size ratios have little effect on the wettability of the droplets, and the theoretical results are in good agreement with the experimental ones. Figure 6b plots the relationship between b/a and θ in which S/D_b = 1. Taking the average value and assuming that b/a = 0.75 in the experiment of Liu et al.[34] and b/a = 1 in this paper, the theoretical results are in good agreement with the experimental ones. Generally speaking, S/D_b < 2.2 and 0.4 < b/a < 2.2 when S/D_b = 1 are required in order to make the surface superhydrophobic and keep droplets in the Lotus effect region so that the viscous resistance they suffer during the rebound stage is reduced.

The Phase Diagram and the Contact Time of Pancake Bouncing. The range of microstructure size and contact time of droplets required for pancake bouncing were further analyzed. The pointed line, dash-dotted line, and dashed line in Figure 7 represent the appropriate wetting states, energy

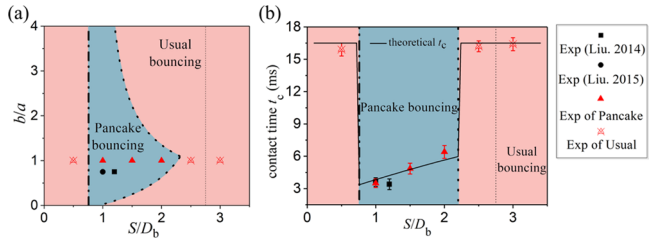

Figure 7. (a) Phase diagram showing the range of pancake bouncing and the effect of the ratio S/D_b of the conical array and the ratio of the nanosphere structures b/a on pancake bouncing. R_0 = 1.45 mm and We ≈ 16. (b) Relationship between the contact time t_c of the droplets and the array spacing S/D_b under pancake bouncing conditions. The ratio of the nanosphere structures b/a = 1, R_0 = 1.45 mm, and We ≈ 16. The pointed line represents the appropriate wetting states $S/D_b \leq 2.2$ when b/a = 1, as shown in Figure 2a, the dash-dotted line represents the energy criterion (based on Equation 7) when $S/D_b \geq 0.76$, and the dashed lines represent the comparable timescales k when $0 \leq S/D_b \leq 2.75$ for pancake bouncing.

criterion, and comparable timescales for pancake bouncing, respectively. As can be seen from Figure 7a, the ratio of the nanosphere (b/a) in the range between 0.5 and 1.5 has little effect on the energy storage of the droplets, but the wetting state range is greatest at these sizes. For the conical arrays, a very small S/D_b results in insufficient energy storage, and no pancake bouncing occurs. The reason is that the spaces between the posts are too dense, and the penetration depth of the liquid is not enough to store rebound energy. Similarly, when the ratio of the conical arrays S/D_b exceeds 2, the droplets will not be able to conduct the pancake bounce due to being in the CB–W area. The black solid points in Figure 7a are the points at which the pancake bouncing occurred in previously reported experiments.[34,44] They are located in the theoretical region of pancake bouncing (the blue region). Furthermore, for a droplet impacting on the SCAS, in this case, the comparable timescale does not limit the pancake bouncing of the droplets, as indicated by the dashed lines in the figure.

DOI: 10.1021/acs.langmuir.9b03153
Langmuir 2019, 35, 17000–17008

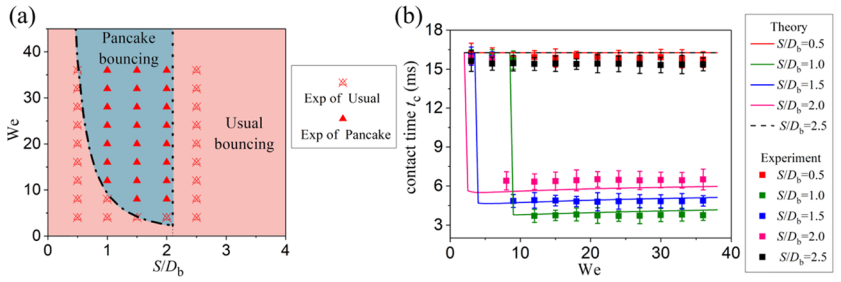

Figure 8. (a) Phase diagram showing the range of bouncing states of a droplet (R_0 = 1.45 mm) rebounded under different S/D_b and We under the limitations of the pancake bouncing. The pointed line represents the appropriate wetting states $S/D_b \leq 2.2$ when $b/a = 1$, as shown in Figure 2a, and the dash-dotted line represents the energy criterion for pancake bouncing. (b) Rebound situation of the droplets (R_0 = 1.45 mm) under a different Weber number We of the SCAS with $b/a = 1$.

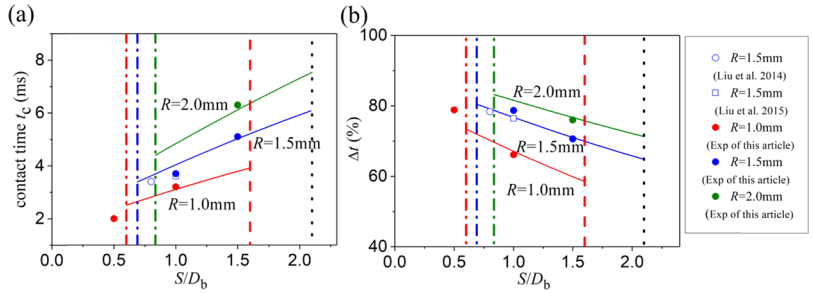

Figure 9. Variation of (a) the contact time t_c and (b) the degree of shortening of the contact time Δt according to the ratio of the conical arrays and the radii of the droplets at $We \approx 20$. The red, blue, and green dash-dotted lines represent the energy criterion of R_0 = 1.0 mm, R_0 = 1.5 mm, and R_0 = 2.0 mm, respectively. The pointed line represents the appropriate wetting states $S/D_b \leq 2.2$ when $b/a = 1$, as shown in Figure 2a; the red dashed line represents the comparable timescales k of R_0 = 1.0 mm.

Points at which pancake bouncing does not occur are located in the normal bouncing area (the red region). Figure 7b shows the effect of the microstructure size on droplet contact time for We = 16. The triangular points are experimental values, and the red area indicates the portion where the droplet cannot rebound like a pancake. The contact time of normal bouncing droplets is approximately 16.5 ms. But for pancake bouncing, the contact time of the droplets is much smaller than that of normal bouncing droplets and increases with an increase in microstructure spacing (3.35 to 5.97 ms).

Next, in order to reveal the effect of the impact energy of the droplet (herein indicated by the Weber number We) on pancake bouncing, a nanosphere structure ($b/a = 1$) is used, as shown in Figure 8a. Due to the limitations of the wetting states, pancake bouncing cannot occur in the area where $S/D_b > 2.2$. When the size of the spacing is reduced, a larger We is required to allow the droplets to store enough rebound energy. For the SCAS with an array spacing of $S/D_b \approx 0.5$, the droplets require substantial initial kinetic energy for pancake bouncing. Therefore, increasing the spacing between the posts is conducive to increasing energy storage, which is beneficial to pancake bouncing. Figure 8b presents the relationship between the contact time of the droplets, We, and the spacing of the microstructures. For the surface with a conical array ratio of S/D_b = 0.5 and S/D_b = 2.5, due to the conditional limitations of pancake bouncing, the droplets rebound as normal, and the contact time is independent of We, which is approximately 16.5 ms. However, for the surface with S/D_b = 1 when We = 9, the droplet will rebound from the surface in the form of a pancake, and the contact time is sharply reduced to approximately 3.7 ms. In addition, as the spacing increases, the We required for the pancake bouncing of the droplet will be reduced. In contrast, the contact time t_c of the pancake bouncing will increase. For the surface with S/D_b = 2, pancake bouncing requires only We = 2.5, but the contact time increases to 5.6–5.9 ms. $t_\uparrow$ is related to the impact velocity v_0 (based on Equation 9), and t_c is fixed over the pancake bouncing range. Specific images are demonstrated in the C2 section in the Supporting Informations.

The Effect of the Droplet Size on the Rebound. The above studies are based on a droplet radius of R_0 = 1.45 mm. However, the size of the droplet will also affect pancake bouncing. In order to determine the relationship between the size of the droplet and pancake bouncing, we conducted an experiment on the rebounding of droplets on a surface with S/D_b = 1, as shown in Figure S4 in the Supporting Information. In the case where the droplet volume is too small ($V \leq 3$ μL) or too large ($V \geq 75$ μL), pancake bouncing cannot occur due to the unfavorable timescales. When the volume of the droplet is at 5 μL $\leq V \leq$ 50 μL, the pancake bouncing phenomenon can be clearly observed, and the contact time t_c increases as the droplet volume increases. Additionally, we also conducted an experimental study concerning the rebounding of droplets on surfaces of S/D_b = 0.5, S/D_b = 1.0, and S/D_b = 1.5 (specific information is demonstrated in Figure S5 in the Supporting Information). The effect of the size of the droplets and microstructure size on the pancake bouncing can be seen in Figure S6 in the Supporting Information. In order to facilitate the observation, the radius of the droplet is obtained via its volume, giving a We value of 20. It can be seen that as the spacing of the conical array increases, the pancake bouncing range of the droplets also gradually increases. In addition, a dimensional effect between the droplet and the microstructure can be observed. The pancake bouncing would be more likely to happen on the surfaces with large post spacing for the droplet with the larger radius (Figure S6).

DOI: 10.1021/acs.langmuir.9b03153
Langmuir 2019, 35, 17000−17008

By above results analysis, a relationship between the contact time t_c of the droplets, the droplet's size R_0, and the spacing of the microstructures S/D_b is obtained as shown in Figure 9, which is a good linear relationship between the contact time t_c of the droplets and the size of the microstructures. As a result, for a droplet with radius R = 1 mm, the microstructure size on which pancake bouncing can occur is in the range of $0.6 < S/D_b < 1.6$. The contact time of the experiment can be shortened to 2 ms. Relating the contact time when the droplets are pancake bouncing (t_c) and bouncing normally (t_c'), the degree of the shortening of the contact time can be obtained with $\Delta t = (t_c' - t_c)/t_c'$. The relationship between the reduction in the contact time of impacting droplets and the size of the microstructures on the SCAS is displayed in Figure 9b. The dash-dotted lines of different colors on the graph indicate the minimum microstructure spacing on which pancake bouncing will occur. The uncolored points on the graph represent the data from previous experiments and the colored points represent the results obtained from our experiments in this work. The result implies that the pancake bouncing of droplets has a dimensional effect. For droplets with different radii, the maximum reduction of the contact times Δt is very similar, approximately 83.2%. In our experiments, the rebounding time of the droplets is reduced by nearly 80%, approaching the theoretical limit.

In addition to the above factors, the half apex angle α of microstructures also affects the rebounding of droplets. For the microstructures with a top surface diameter D_b = 100 μm and column height H = 600 μm, as shown in Figure S7 in the Supporting Information, with the increase of the α, the size spacing range of pancake bounce increases because the increased α is beneficial to the storage of the droplet rebound energy.

CONCLUSIONS

In summary, we have investigated the phenomenon of the pancake bouncing of droplets on a superhydrophobic conical array surface. First, the dynamic wetting states of the droplets were studied theoretically and experimentally. Second, we theoretically obtained a droplet bounce phase diagram, determined the droplet contact time on the superhydrophobic conical array, and concluded that the elastic energy and contact time could be adjusted by altering the size of the microstructures. Furthermore, the influence of droplet size and conical microstructural spacing on droplet resilience was analyzed, and a quantitative relationship between the droplet volume and conical microstructural spacing was determined. It is believed that our studies will allow for the reasonable design of surfaces for many practical applications in the future.

ASSOCIATED CONTENT

Supporting Information

The Supporting Information is available free of charge at https://pubs.acs.org/doi/10.1021/acs.langmuir.9b03153.

C1 showing the wetting states of a droplet on the SCAS, C2 showing the bouncing states of a droplet on the SCAS, C3 showing the relationship between droplet size and its rebound states, and C4 showing the relationship between the spacing of the conical arrays S/D_b and half apex angle α (PDF)

Video S1 showing the rebounding of a droplet on the SCAS with S/D_b = 0.5 (AVI)

Video S2 showing the rebounding of a droplet on the SCAS with S/D_b = 1.0 (AVI)

Video S3 showing the rebounding of a droplet on the SCAS with S/D_b = 1.5 (AVI)

Video S4 showing the rebounding of a droplet on the SCAS with S/D_b = 2.0 (AVI)

Video S5 showing the rebounding of a droplet on the SCAS with S/D_b = 2.5 (AVI)

AUTHOR INFORMATION

Corresponding Author

*Email: wuhuaping@gmail.com.

ORCID

Huaping Wu: 0000-0003-4505-7062

Hao Bai: 0000-0002-3348-6129

Aiping Liu: 0000-0002-2338-062X

Notes

The authors declare no competing financial interest.

ACKNOWLEDGMENTS

This work was supported by the National Science Foundation of China (grant nos. 11672269, 11972323, 51572242, and 51675485), the Zhejiang Provincial Natural Science Foundation of China (grant nos. LR20A020002, LR19E020004, and LR18E050002), and the Fundamental Research Funds for the Provincial Universities of Zhejiang (RF-B2019004).

REFERENCES

(1) Antonini, C.; Jung, S.; Wetzel, A.; Heer, E.; Schoch, P.; Moqaddam, A. M.; Chikatamarla, S. S.; Karlin, I.; Marengo, M.; Poulikakos, D. Contactless Prompt Tumbling Rebound of Drops From a Sublimating Slope. *Phys. Rev. Fluids* **2016**, *1*, No. 013903.

(2) Yan, X.; Zhang, L.; Sett, S.; Feng, L.; Zhao, C.; Huang, Z.; Vahabi, H.; Kota, A. K.; Chen, F.; Miljkovic, N. Droplet Jumping: Effects of Droplet Size, Surface Structure, Pinning, and Liquid Properties. *ACS Nano* **2019**, *13*, 1309−1323.

(3) Song, D.; Song, B.; Hu, H.; Du, X.; Ma, Z. Contact Angle and Impinging Process of Droplets on Partially Grooved Hydrophobic Surfaces. *Appl. Therm. Eng.* **2015**, *85*, 356−364.

(4) Wu, H.; Zhu, K.; Cao, B.; Zhang, Z.; Wu, B.; Liang, L.; Chai, G.; Liu, A. Smart Design of Wettability-Patterned Gradients on Substrate-Independent Coated Surfaces to Control Unidirectional Spreading of Droplets. *Soft Matter* **2017**, *13*, 2995−3002.

(5) Zhang, H.; Yi, X.; Du, Y.; Zhang, R.; Zhang, X.; He, F.; Niu, F.; Hao, P. Dynamic Behavior of Water Drops Impacting on Cylindrical Superhydrophobic Surfaces. *Phys. Fluids* **2019**, *31*, No. 032104.

(6) Weisensee, P. B.; Tian, J.; Miljkovic, N.; King, W. P. Water Droplet Impact on Elastic Superhydrophobic Surfaces. *Sci. Rep.* **2016**, *6*, 30328.

(7) Davis, A.; Surdo, S.; Caputo, G.; Bayer, I. S.; Athanassiou, A. Environmentally Benign Production of Stretchable and Robust Superhydrophobic Silicone Monoliths. *ACS Appl. Mater. Interfaces* **2018**, *10*, 2907−2917.

(8) Zhang, J.; Gu, C.; Yan, W.; Tu, J.; Ding, X. Fabrication and corrosion property of conversion films on magnesium alloy from deep eutectic solvent. *Surf. Coat. Technol.* **2018**, *344*, 702−709.

(9) Wang, L.; Gong, Q.; Zhan, S.; Jiang, L.; Zheng, Y. Robust Anti-Icing Performance of a Flexible Superhydrophobic Surface. *Adv. Mater.* **2016**, *28*, 7729−7735.

(10) Yu, Y. S.; Wang, M. C.; Huang, X. Evaporative Deposition of Polystyrene Microparticles on PDMS Surface. *Sci. Rep.* **2017**, *7*, 14118.

(11) Wang, Y.; Xue, J.; Wang, Q.; Chen, Q.; Ding, J. Verification of Icephobic/Anti-icing Properties of a Superhydrophobic Surface. *ACS Appl. Mater. Interfaces* **2013**, *5*, 3370−3381.

DOI: 10.1021/acs.langmuir.9b03153
Langmuir 2019, 35, 17000−17008

(12) Qiu, X.; Yang, Z.; Wu, H.; Guo, J.; Zhang, Z.; Feng, J.; Chai, G.; Liu, A. Excellent Oil-Water Separation Under External Pressure: Controllable Critical Pressure and Separation Efficiency by Well-Designed Hierarchical Mesh Structure. *Appl. Surf. Sci.* **2018**, *456*, 602−608.
(13) Cui, Y.; Li, Y.; Xing, Y. Sweat Effects on The Thermal Analysis of Epidermal Electronic Devices Integrated with Human Skin. *Int. J. Heat Mass Transfer* **2018**, *127*, 97−104.
(14) Zhang, J.; Lin, W.; Zhu, C.; Lv, J.; Zhang, W.; Feng, J. Dark, Infrared Reflective, and Superhydrophobic Coatings by Waterborne Resins. *Langmuir* **2018**, *34*, 5600−5605.
(15) Lee, S.-H.; Seong, M.; Kwak, M. K.; Ko, H.; Kang, M.; Park, H. W.; Jeong, H. E. Tunable Multimodal Drop Bouncing Dynamics and Anti-Icing Performance of a Magnetically Responsive Hair Array. *ACS Nano* **2018**, *12*, 10693−10702.
(16) Zhang, S.; Huang, J.; Chen, Z.; Yang, S.; Lai, Y. Liquid Mobility on Superwettable Surfaces for Applications in Energy and the Environment. *J. Mater. Chem. A* **2019**, *7*, 38−63.
(17) Tong, W.; Xiong, D.; Wang, N.; Yan, C.; Tian, T. Green and Timesaving Fabrication of A Superhydrophobic Surface and its Application to Anti-icing, Self-cleaning and Oil-water Separation. *Surf. Coat. Technol.* **2018**, *352*, 609−618.
(18) Liu, X.; Chen, H.; Zhao, Z.; Wang, Y.; Liu, H.; Zhang, D. Self-jumping Mechanism of Melting Frost on Superhydrophobic Surfaces. *Sci. Rep.* **2017**, *7*, 14722.
(19) Xie, Y.; Chen, H.; Shen, Y.; Tao, J.; Jin, M.; Wu, Y.; Hou, W. Rational Fabrication of Superhydrophobic Nanocone Surface for Dynamic Water Repellency and Anti-icing Potential. *J. Bionic Eng.* **2019**, *16*, 27−37.
(20) Li, H.; Fang, W.; Li, Y.; Yang, Q.; Li, M.; Li, Q.; Feng, X.-Q.; Song, Y. Spontaneous Droplets Gyrating via Asymmetric Self-splitting on Heterogeneous Surfaces. *Nat. Commun.* **2019**, *10*, 950.
(21) Zang, D.; Wang, X.; Geng, X.; Zhang, Y.; Chen, Y. Impact Dynamics of Droplets With Silica Nanoparticles and Polymer Additives. *Soft Matter* **2013**, *9*, 394−400.
(22) Josserand, C.; Thoroddsen, S. T. Drop Impact on a Solid Surface. *Annu. Rev. Fluid Mech.* **2016**, *48*, 365−391.
(23) Han, J.; Ryu, S.; Kim, H.; Sen, P.; Choi, D.; Nam, Y.; Lee, C. Anisotropic Drop Spreading on Superhydrophobic Grates During Drop Impact. *Soft Matter* **2018**, *14*, 3760−3767.
(24) Mulroe, M. D.; Srijanto, B. R.; Ahmadi, S. F.; Collier, C. P.; Boreyko, J. B. Tuning Superhydrophobic Nanostructures to Enhance Jumping-droplet Condensation. *ACS Nano* **2017**, *11*, 8499−8510.
(25) Malla, L. K.; Patil, N. D.; Bhardwaj, R.; Neild, A. Droplet Bouncing and Breakup during Impact on a Microgrooved Surface. *Langmuir* **2017**, *33*, 9620−9631.
(26) Richard, D.; Clanet, C.; Quéré, D. Contact time of a bouncing drop. *Nature* **2002**, *417*, 811.
(27) Lv, C.; Hao, P.; Zhang, X.; He, F. Drop Impact Upon Superhydrophobic Surfaces with Regular and Hierarchical Roughness. *Appl. Phys. Lett.* **2016**, *108*, 141602.
(28) Hao, C.; Li, J.; Liu, Y.; Zhou, X.; Liu, Y.; Liu, R.; Che, L.; Zhou, W.; Sun, D.; Li, L.; Xu, L.; Wang, Z. Superhydrophobic-like Tunable Droplet Bouncing on Slippery Liquid Interfaces. *Nat. Commun.* **2015**, *6*, 7986.
(29) Bird, J. C.; Dhiman, R.; Kwon, H. M.; Varanasi, K. K. Reducing the Contact Time of a Bouncing Drop. *Nature* **2013**, *503*, 385−388.
(30) Gauthier, A.; Symon, S.; Clanet, C.; Quéré, D. Water Impacting on Superhydrophobic Macrotextures. *Nat. Commun.* **2015**, *6*, 8001.
(31) Shen, Y.; Tao, J.; Tao, H.; Chen, S.; Pan, L.; Wang, T. Approaching the Theoretical Contact Time of a Bouncing Droplet on the Rational Macrostructured Superhydrophobic Surfaces. *Appl. Phys. Lett.* **2015**, *107*, 111604.
(32) Liu, Y.; Andrew, M.; Li, J.; Yeomans, J. M.; Wang, Z. Symmetry Breaking in Drop Bouncing on Curved Surfaces. *Nat. Commun.* **2015**, *6*, 10034.
(33) Chen, S.; Bertola, V. Drop Impact on Spherical Soft Surfaces. *Phys. Fluids* **2017**, *29*, No. 082106.
(34) Liu, Y.; Moevius, L.; Xu, X.; Qian, T.; Yeomans, J. M.; Wang, Z. Pancake Bouncing on Superhydrophobic Surfaces. *Nat. Phys.* **2014**, *10*, 515−519.
(35) Song, J.; Gao, M.; Zhao, C.; Lu, Y.; Huang, L.; Liu, X.; Carmalt, C. J.; Deng, X.; Parkin, I. P. Large-Area Fabrication of Droplet Pancake Bouncing Surface and Control of Bouncing State. *ACS Nano* **2017**, *11*, 9259−9267.
(36) Guo, C.; Zhao, D.; Sun, Y.; Wang, M.; Liu, Y. Droplet Impact on Anisotropic Superhydrophobic Surfaces. *Langmuir* **2018**, *34*, 3533−3540.
(37) Kumar, A.; Tripathy, A.; Nam, Y.; Lee, C.; Sen, P. Effect of Geometrical Parameters on Rebound of Impacting Droplets on Leaky Superhydrophobic Meshes. *Soft Matter* **2018**, *14*, 1571−1580.
(38) Bro, J. A.; Jensen, K. S. B.; Larsen, A. N.; Yeomans, J. M.; Hecksher, T. The Macroscopic Pancake Bounce. *Eur. J. Phys.* **2017**, *38*, No. 015006.
(39) Wu, H.; Yu, S.; Xu, Z.; Cao, B.; Peng, X.; Zhang, Z.; Chai, G.; Liu, A. Theoretical and Experimental Study of Reversible and Stable Wetting States of a Hierarchically Wrinkled Surface Tuned by Mechanical Strain. *Langmuir* **2019**, *35*, 6870−6877.
(40) Graeber, G.; Martin Kieliger, O. B.; Schutzius, T. M.; Poulikakos, D. 3D-Printed Surface Architecture Enhancing Superhydrophobicity and Viscous Droplet Repellency. *ACS Appl. Mater. Interfaces* **2018**, *10*, 43275−43281.
(41) Liu, Y.; Wang, Z. Superhydrophobic Porous Networks for Enhanced Droplet Shedding. *Sci. Rep.* **2016**, *6*, 33817.
(42) Dong, X.; Huang, X.; Liu, J. Modeling and Simulation of Droplet Impact on Elastic Beams Based on SPH. *Eur. J. Mech. A-Solids.* **2019**, *75*, 237−257.
(43) Liu, J.; Mei, Y.; Xia, R. A New Wetting Mechanism Based upon Triple Contact Line Pinning. *Langmuir* **2011**, *27*, 196−200.
(44) Liu, Y.; Mhyman, G.; Bormashenko, E.; Hao, C.; Wang, Z. Controlling Drop Bouncing Using Surfaces with Gradient Features. *Appl. Phys. Lett.* **2015**, *107*, No. 051604.
(45) Moevius, L.; Liu, Y.; Wang, Z.; Yeomans, J. M. Pancake Bouncing: Simulations and Theory and Experimental Verification. *Langmuir* **2014**, *30*, 13021−13032.
(46) Moqaddam, A. M.; Chikatamarla, S. S.; Karlin, I. V. Drops Bouncing Off Macro-textured Superhydrophobic Surfaces. *J. Fluid Mech.* **2017**, *824*, 866−885.
(47) Wu, H.; Zhu, K.; Wu, B.; Lou, J.; Zhang, Z.; Chai, G. Influence of Structured Sidewalls on the Wetting States and Superhydrophobic Stability of Surfaces with Dual-scale Roughness. *Appl. Surf. Sci.* **2016**, *382*, 111−120.
(48) Wu, H.; Yang, Z.; Cao, B.; Zhang, Z.; Zhu, K.; Wu, B.; Jiang, S.; Chai, G. Wetting and Dewetting Transitions on Submerged Superhydrophobic Surfaces with Hierarchical Structures. *Langmuir* **2017**, *33*, 407−416.
(49) Feng, L.; Zhang, Y. A.; Xi, J. M.; Zhu, Y.; Wang, N.; Xia, F.; Jiang, L. Petal Effect: A Superhydrophobic State with High Adhesive Force. *Langmuir* **2008**, *24*, 4114−4119.
(50) Laan, N.; de Bruin, K. G.; Bartolo, D.; Josserand, C.; Bonn, D. Maximum Diameter of Impacting Liquid Droplets. *Phys. Rev. Appl.* **2014**, *2*, No. 044018.
(51) Clanet, C.; Béguin, C.; Richard, D.; Quéré, D. Maximal Deformation of An Impacting Drop. *J. Fluid Mech.* **1999**, *517*, 199−208.
(52) Hasimoto, H. On the Periodic Fundamental Solutions of the Stokes Equations and Their Application to Viscous Flow Past a Cubic Array of Spheres. *J. Fluid Mech.* **1959**, *5*, 317−328.
(53) Ishino, C.; Reyssat, M.; Reyssat, E.; Okumura, K.; Quéré, D. Wicking Within Forests of Micropillars. *Europhys. Lett.* **2007**, *79*, 56005.
(54) Pasandideh-Fard, M.; Qiao, Y. M.; Chandra, S.; Mostaghimi, J. Capillary Effects during Droplet Impact on a Solid Surface. *Phys. Fluids* **1996**, *8*, 650−659.
(55) Bartolo, D.; Bouamrirene, F.; Verneuil, É.; Buguin, A.; Silberzan, P.; Moulinet, S. Bouncing or Sticky Droplets: Impalement

DOI: 10.1021/acs.langmuir.9b03153
Langmuir 2019, 35, 17000−17008

Transitions on Superhydrophobic Micropatterned Surfaces. *Europhys. Lett.* **2006**, *74*, 299.

DOI: 10.1021/acs.langmuir.9b03153
Langmuir 2019, 35, 17000−17008